MRI-VisAct: A Bowden Cable-driven MRI Compatible Series Viscoelastic Actuator

Yusuf Mert Senturk and Volkan Patoglu

Abstract

Presence of the strong magnetic fields in the Magnetic Resonance Imaging (MRI) environment limits the integration of robotic rehabilitation systems to the MRI process. The tendency to improve imaging quality by the amplification of magnetic field strength further tightens the bidirectional compatibility constraints on MRI compatible rehabilitation devices. We present the design, control, and characterization of *MRI-VisAct*—a low-cost, Bowden cable-actuated rotary series viscoelastic actuator that fulfills the bidirectional compatibility requirements to the maximum extend. Components of *MRI-VisAct* that are placed in the magnet room are built using nonconductive, diamagnetic MRI compatible materials, while ferromagnetic/paramagnetic components are placed in the control room, located outside the MRI room. Power and data transmission are achieved through Bowden-cables and fiber optics, respectively. This arrangement ensures that neuroimaging artifacts are minimized, while safety hazards are eliminated, and the device performance is not affected by the magnetic field. *MRI-VisAct* works under closed-loop torque control enabled through series viscoelastic actuation. *MRI-VisAct* is fully customizable; it can serve as the building block of higher degrees of freedom MRI compatible robotic devices.

Keywords

MRI compatible robots, rehabilitation robotics, bidirectional compatibility, series elastic actuation, physical human-robot interaction

Introduction

Physical therapies are indispensable for treatment of neurological problems. Therapies are conventionally delivered via physiotherapists who provide active assistance and/or guidance to patients to help promote recovery by fulfilling a set of exercises. The amount of manual labor involved in conventional physiotherapy is a major concern, especially when considered in relation to the aging trend of world's population in developed countries (Lutz and Scherbov 2008).

Advanced age is known to be one of the leading causes of stroke, a major generator of motor function deficiency (Wolf et al. 1991). Aging population is expected to generate a larger gap between supply and demand of human labor in the field physiotherapy. Along these lines, robot-assisted rehabilitation systems are becoming essential parts of physical therapy. In addition to reducing the manual work load on therapists, rehabilitation robots also serve to improve the standardization and repeatability of exercises during therapy sessions, and provide quantitative measurements of patient performance.

Many robotic rehabilitation devices are being employed for treatment of a range of neurological problems, including treating joint instability, inability to bear weight, and loss of limb function. With the proliferation of robotic rehabilitation systems, recent efforts have concentrated on improving efficacy of therapies conducted through use of such devices. Given that neuroplasticity of the brain is considered as the main mechanism driving recovery, neuroimaging techniques can provide decisive information to evaluate efficacy of different treatment procedures (Dong et al. 2006).

Among the non-invasive diagnostic methods for imaging the brain, Magnetic Resonance Imaging (MRI) is one of the most preferred ones. Functional MRI (fMRI), a procedure in MRI studies, measures brain activity associated with blood flow. In particular, activation in an area of the brain causes flow of oxygenated blood cells to that part of the brain to replace deoxigenated ones that display paramagnetic properties

Faculty of Engineering and Natural Sciences, Sabancı University, İstanbul, Turkey.

Corresponding author:
Volkan Patoglu, Faculty of Engineering and Natural Sciences, Sabancı University, 34956, İstanbul, Turkey.
Email: vpatoglu@sabanciuniv.edu

and interfere with magnetic signals of the MRI machine. Because of this phenomena, the activated regions of the brain appear comparatively brighter in MRI scans.

If the rehabilitation devices can be operated during fMRI, the activation of regions in sensory-motor cortex can be studied during therapies and conclusions about the effectiveness of different rehabilitation treatments can be made. Therefore, fMRI compatible rehabilitation devices can lead to evidence-based robotic rehabilitation treatments that are personalized according to the personal needs of each patient and structured to achieve maximum efficacy.

Although the potential of such studies are great, the adaption of classical rehabilitation devices into MRI environments is not a trivial task. The design of such devices should comply with the narrow dimensions of MRI machines and also ensure successful operation under the presence of strong magnetic fields. For successful operation of a device during MRI, it should satisfy two crucial constraints, which are together named as bidirectional compatibility constraints.

First constraint is to ensure successful realization of MRI procedures without any interference from the device. For this, the device should, not only not cause any safety hazards for the patient and environment, but also not create any disturbances to the quality of images. This compatibility requirement limits the use of standard actuation methodologies, like direct current motors. Similarly utilization of any ferromagnetic material should be avoided, due to their high magnetic susceptibility, as they may cause strong magnetic forces to be induced, leading to missile effect. Another safety hazard can be caused by the heating of conductive materials due to the eddy currents that develop on them because of the changing magnetic fields. These currents may cause excessive temperature elevations in these parts. In addition to these safety hazards, any other type of actuation and sensing mechanism that contains electric circuitry is not preferred, due to the external magnetic effects and radio frequency interference that it may create. These type of parasitic effects are known to present themselves in the MR images as false positive activation artifacts, spatial distortion, and shading.

Second condition of compatibility with MRI requires that the performance of the device should not be hindered by the high magnetic field of the MRI machine. Actuators and sensors that employ means of

electrical actuation and reading are disturbed by the eddy current effects caused by the changing magnetic fields of the MRI machine. Similarly, sensor readings can be distorted by heating of the sensors due to the same effects (Gassert et al. 2008).

The strength of the magnetic field generated during fMRI studies is closely related, not only to the imaging quality and the length of image acquisition protocols, but also to the compatibility of mechatronic devices that are used during these procedures. As MRI technology goes forward, the field strength of the MRI machines also increases. For example, while first MRI magnets operated at 0.1 T to 0.3 T, currently the most of the commercial devices operate at 1.5 T to 3 T levels (Le Bihan 2014). Since higher magnetic fields are preferred for high quality neuroimaging, the bidirectional compatibility requirements are likely to become more challenging in the near future with the spread of machines that use 7 T or higher magnetic field strengths. Such MRI machines are currently being used for research (Budinger and Bird 2017).

We propose *MRI-VisAct*, a low-cost, force-controlled MRI compatible actuator that features ideal bidirectional compatibility, to future-proof robot-assisted rehabilitation protocols within MRI. The proposed actuator does not utilize any conductive material or electric circuitry inside the MRI room and can deliver good torque control performance for safe and effective delivery of robot-assisted rehabilitation.

The rest of the paper is organized as follows: Related Work section provides a comprehensive literature review of MRI compatible devices and outlines the novel aspects of *MRI-VisAct*. Design Requirements section reviews the constraints imposed on the design MRI compatible devices, emphasizing the importance of bidirectional compatibility. Design and Implementation section presents the mechatronics design and implementation details of the series viscoelastic element, MRI compatible fiber optic encoders, sensor processing unit, and actuation unit of *MRI-VisAct*. Series Elastic Actuation and Torque Control section reviews series elastic actuation, viscoelastic modeling, and introduces control architecture of the device. Experimental Characterization and Verification section provides comprehensive evaluation of device performance. Finally, Discussion and Conclusion section provides an overall evaluation of the proposed approaches.

Table 1. A list of MRI Compatible Human Movement Pattern/Rehabilitation Assessment Devices

	Actuation Type	Force Sensing	Position Sensing	Application
	Mechanisms Present in the MRI Room			
Reference	**Actuation Type**	**Force Sensing**	**Position Sensing**	**Application**
(Hidler et al. 2006)	No actuation	Non-magnetic 6-axis load cell	-	Wrist force/moment measurements
(Newton et al. 2008)	No actuation	Non-magnetic 6-axis load cell	-	Ankle, knee and hip torque measurements
(Mehta et al. 2009)	No actuation	-	Optical encoder	Pedaling speed measurements
(Sergi et al. 2011)	No actuation	-	Optical encoders	Post rehabilitation efficacy prediction
(Menon et al. 2014)	Particle-jamming via pneumatic actuation	-	-	Mechanical modulation of device stiffness
(Khanicheh et al. 2008)	ERF actuation	Aluminum strain gage	Optical encoders	Mechanical modulation of device damping
(Hara et al. 2009)	Electrostatic motors	Non-magnetic force sensor	Synchronous drive	2-Dof motion & force rendering joystick
(Hollnagel et al. 2011)	Pneumatic actuation	Resistive strain gauges	Optical encoder, foil potentiometer	Analysis of stepping patterns
(Gassert et al. 2006)	Hydraulic actuation	Fiber optic force sensors	Shielded optical encoders	Analysis of reaching movements
(Yu et al. 2008)	Pneumatic actuation hydraulic actuation	Optical force sensors	Optical encoders, potentiometers	Comparison of hydraulic and pneumatic actuation
(Ergin et al. 2014)	Ultrasonic motors	Shielded aluminum strain gage	Optical encoders	Analysis of pick & place movements
(Sergi et al. 2015)	Series elastic actuation with ultrasonic motors	Series elastic force sensing	Optical encoders	Torque controlled wrist rehabilitation
(Li et al. 2009)	Shielded DC motors with cable transmission through carbonfiber rods	DC motors	Optical encoder	Analysis of hand movements
(Chapuis et al. 2006)	DC Motor Cable Transmission	Fiber optic force sensor	Optical encoder	Investigation of cable transmission for MRI
(Menon et al. 2016)	Shielded DC motors & transmission using rods	DC motors	Optical encoders	Analysis of haptic perception, motor control
MRI-VisAct (2017)	Series viscoelastic actuation with Bowden-cables	Fiber optic force sensing via series elasticity	Fiber optic encoders	Administering torque controlled rehabilitation exercises

Related Work

MRI compatible mechatronic devices have been used for several applications, such as surgery, analysis of haptic perception, and rehabilitation. Researchers have proposed various design approaches to address the design challenges induced by harsh compatibility constraints to enable robot-assisted rehabilitation in MR environments. Table 1 summarizes MRI compatible rehabilitation devices in the literature. These devices can be loosely categorized according to their actuation scheme as follows:

The first category belongs to devices with no actuation (Hidler et al. 2006; Newton et al. 2008; Mehta et al. 2009). The purpose of these devices is to measure the interaction forces or movement patterns of patients during, just before, or just after the MRI process. The devices in this category are typically equipped with multi degrees of freedom force sensors or optical encoders that are MRI compatible. Although these devices help researchers gather data for perception and diagnostic studies, their use for rehabilitation is limited due to their inability to assist patients.

The second category of devices are the ones that are capable of passive modulation of their impedance through unconventional techniques, such as particle jamming (Khanicheh et al. 2008) or electro-rheological fluidics (ERF) (Menon et al. 2014). Even though these devices are capable of stiffness and/or damping modulation, their adaptation for rehabilitation stays limited as these devices are also incapable of providing active assistance to patients.

The third category includes devices that are actuated with MRI compatible electro-static motors (Hara et al. 2009). Electro-static motors use electrical fields for actuation, where the actuator performance depends heavily on the current flowing inside them. Large electrical currents introduce noise to the environment that may interfere with MR images; hence, electro-static motors need to be placed at a certain distance from the MRI machine (Yamamoto et al. 2005).

Devices that use pneumatic actuation belong to the fourth category. Pneumatic actuation relies on compression of intermediate matter to transfer motion and force between a master system outside of the MRI room and a slave system inside the MRI room. This type of actuation can provide high forces that are adequate for physical rehabilitation and assessment; however, the compressibility of air, pressure losses in piping/valves, and friction in the pistons negatively affects the bandwidth and force control performance of these devices (Yu et al. 2008). The force control performance of these devices stay limited without the introduction of force sensors within the MRI room.

The fifth category consists of devices that utilize hydraulic actuation (Gassert et al. 2006). Due to high friction losses of the hydraulic system, hydraulic actuation requires high internal pressures in the transmission for accurate position control of the system, that lead to bulky structures in the construction of the device. The existence of

high valve friction in hydraulic systems severely limits their use for force controlled physical human-robot interaction.

The devices in the sixth category are actuated with ultrasonic motors (Ergin et al. 2014; Sergi et al. 2015). Ultrasonic motors are MR compatible and possess high output impedance, displaying a good position control performance. However, these actuators are not only of high cost, but also require integration of force sensors for their use in pHRI studies. For instance, in (Sergi et al. 2015), ultrasonic motors have been used with bronze springs acting as series elastic elements to render the overall system into a force controlled series elastic actuator. However, ultrasonic motors inherently contain electric circuitry that introduces noise to the environment and may cause MR image artifacts, especially with the new generation of MRI devices with strong magnetic fields.

The seventh category of devices rely on magnetic shielding to use standard DC motors within the MRI room. In particular, the motors are positioned in Faraday cages such that the MRI compatibility is established up to some extent. However, similar to the case with the electrostatic motors, these systems need be placed a certain distance away from the bore of the MRI machine. Along these lines, both mechanical linkages (Li et al. 2009; Menon et al. 2016) and cable-based transmissions (Spaelter et al. 2006) have been employed for remote location of the actuators. Long linkages and cable-based transmissions both introduce undesired elasticity to the system, and the resulting non-collocation adversely affects the control performance of these approaches. In (Spaelter et al. 2006) a fiber optic force sensor is used to achieve closed-loop force control.

In this paper, we present the design, force control, and experimental characterization of *MRI-VisAct*, a low-cost, Bowden cable-actuated series viscoelastic actuator for robot-assisted physical rehabilitation during MRI. This work significantly extends our earlier feasibility studies presented in (Senturk and Patoglu 2016a,b). Even though Bowden-cable driven series elastic actuation has found use in different force controlled robot-assisted rehabilitation devices (Veneman et al. 2006; Erdogan et al. 2016), none of these designs target MRI compatibility. *MRI-VisAct* is different from these devices in that Bowden-cable actuation is proposed to locate actuation units outside the MRI room, while series viscoelasticity is due to the intentionally introduced nonconductive leaf spring that enable torque estimations force closed loop torque-control.

In particular, *MRI-VisAct* utilizes only nonconductive MRI compatible materials within the MRI room; hence, can provide ideal bidirectional compatibility, unlike any other closed loop force controlled MR compatible rehabilitation devices. To eliminate any imaging artifacts due to the device acting under strong magnetic fields, a Bowden cable-based transmission and custom fiber optic sensing units are introduced. The use of Bowden cable actuation and fiber optic signals enable for the placement of conventional non-MRI compatible control/signal processing units and electric actuators outside the MRI room, as presented in Figure 1, while a series elastic element constructed using polymer leaf springs and fiber optic encoders enable accurate measurement of interaction torques, without causing any interference within the MRI room. The proposed MRI compatible actuator is torque-controlled to enable the control of interaction forces with the patient. The torque control is implemented through a cascaded force-motion control architecture to enable high fidelity control. Furthermore, the proposed device is not only customizable and low cost, but also can act as a building block of higher degrees of freedom MRI compatible robotic devices.
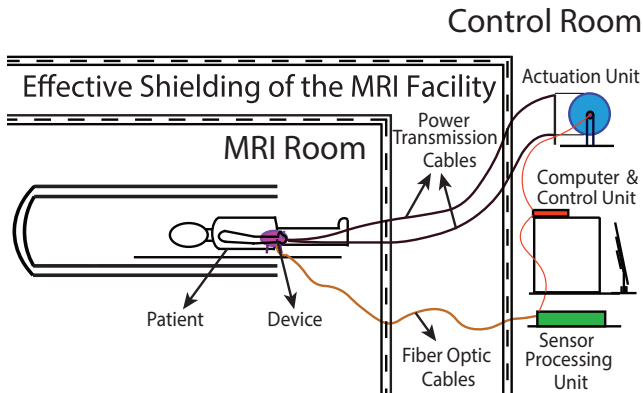

Figure 1. Schematic representation of remote actuator and controller placement, thanks to Bowden cable-based mechanical and fiber optics based signal transmissions

Design Requirements

Even though the overall design is customizable, the MRI compatible actuator presented in this study is designed to deliver single degree

Table 2. Workspace/Torque Limits of Forearm and Wrist (Tsagarakis et al. 1999)

Joint	Human Isometric Strength	Human Joint Workspace Limits
Forearm Supination/Pronation	9.1 Nm (0.02 Nm)	Supination: $86°$ $(86°)$ Pronation: $71°$ $(71°)$
Wrist Flexion/Extension	19.8 Nm (0.5 Nm)	Flexion: $73°$ $(45°)$ Extension: $71°$ $(50°)$
Wrist Radial/Ulnar Deviation	20.8 Nm (0.5 Nm)	Radial Dev.: $19°$ $(19°)$ Ulnar Dev.: $40°$ $(40°)$

Values in parenthesis correspond to the minimal range of motion and torque limits for patients to perform ADL.

of freedom robot-assisted rehabilitation exercises human forearm-wrist joints. Following the terminology of Merlet (Merlet 2006), the performance requirements of the MRI compatible system is categorized into four distinct groups of decreasing importance, namely *imperative*, *optimal*, *primary*, and *secondary* design requirements, as follows:

An imperative design requirement is the kinematic compatibility of the device with the targeted joint. Although the kinematics of human forearm-wrist is coupled and complex, dominant movements can be faithfully modelled as 3 degrees of freedom rotations corresponding to the supination/pronation of forearm, flexion/extension and ulnar/radial deviation of the wrist. The proposed device targets each of these movements independently, by properly aligning the axis of rotation of the device with the corresponding axis of rotation of the relevant joint.

Another imperative design requirement dictates that the device should be capable of delivering physical rehabilitation exercises without sacrificing patient safety. Along these lines, a torque controlled device is designed such that adequate level of interaction forces between the patient and the rehabilitation device can be ensured at all times.

Table 2 presents the workspace and torque output capabilities of the forearm-wrist complex for a healthy human. Since the isometric strength of healthy volunteers is unreasonably high for patients to perform activities of daily living (ADL), the values in the parenthesis, corresponding to the minimal range of motion and torque limits for patients to perform ADL, are provided. The proposed design needs to

ensure that range of motion and torque capabilities of human forearm-wrist for ADL tasks are spanned, by providing a continuous torque output exceeding 0.5 Nm, and a rotary workspace over $\pm 86°$. A motion bandwidth of about 1 Hz is targeted for large rotations to match the human performance within the range of motion. Furthermore, an order of magnitude larger motion bandwidths are necessary for small rotations references that are sufficient to span the allowable deflection range of the elastic element, such that interaction forces can be controlled effective through series elastic actuation.

Considering the technological push to increase the magnetic field strength within MR machines to increase quality of neuroimaging, bidi-rectional compatibility is determined as the optimal design requirement. In particular, bidirectional compatibility should be maximized such that neither the device causes any artifacts in the resulting images, nor the strong magnetic fields interfere with the proper functioning of the device. The proposed device aims at ideal bidirectional compatibility by the use of only strictly MRI compatible, non-conductive materials within the MRI room, and remotely locating actuation and sensor processing units outside the MRI room. Power and data transmission between MRI and control rooms are achieved through Bowden-cables and fiber optics, respectively.

Small device volume and low mass/inertia are considered as primary design requirements, while low cost, compact, and modular design are taken as secondary design requirements.

Design and Implementation

This section details the design and implementation of the mechanical structure, series viscoelastic element, MRI compatible fiber optic encoders, sensor processing and actuation units of *MRI-VisAct*.

Mechanical Design

Mechanical design of *MRI-VisAct* consists of four major plastic parts: support platform, exterior shell, output shaft, and end-effector connectors as presented in Figures 2 and 3. Support platform is grounded to make a $45 \deg$ angle with the horizontal. This angle is chosen in order to enable easier grip of the handle, when the user is lying on his/her back. The main function of the supporting platform is to constrain all unwanted movements due to out of axis forces/torques applied to the system, while
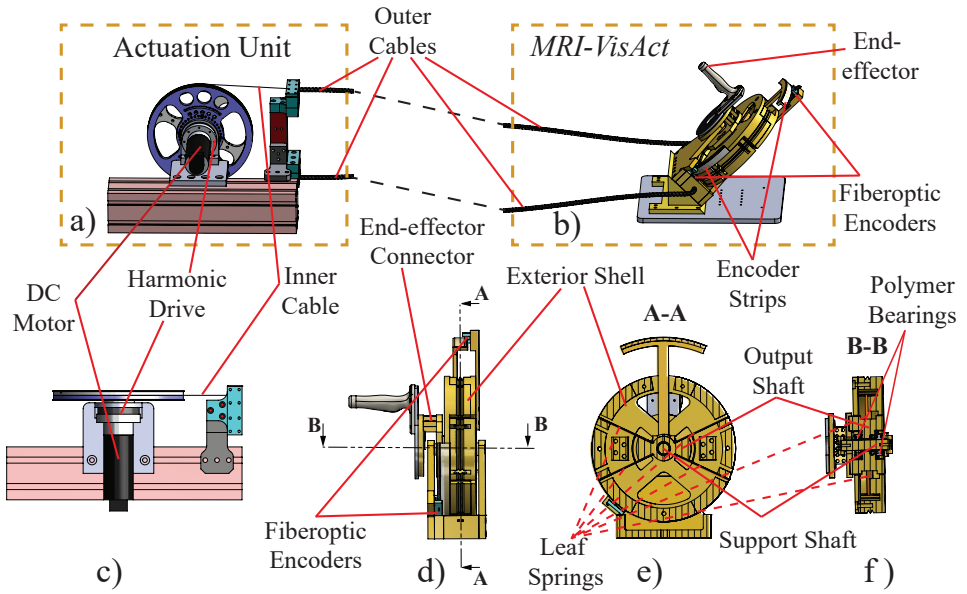
Figure 2. a) Actuation unit located in the control room b) MRI compatible patient interface c) Top-view: Actuation unit d) Side-view: Patient interface, e) and f) Cross-sectional view: Bearings, leaf springs, support and output shafts

also limiting the movements of the cable housing in order to enable the relative motion of the inner cable.

The support platform connects to the exterior shell of the device with the support shaft. MRI compatible polymer glass ball bearings are used between the support shaft and the exterior shell in order to minimize the friction during relative motion. Custom circular grooves are machined on the exterior shell to ensure that the tear-resistant Dyneema ropes are properly coiled up around the exterior shell. Undesired relative motion between the coiled Dyneema ropes and the shell is hindered by screwing the ropes on to the shell via plastic screws.

The exterior shell is connected to the output shaft through four Garolite leaf springs. The output shaft is not mounted on the support shaft, not to induce any parasitic friction. The output shaft can move relative to the exterior shell through deflection of the compliant leaf springs.

Since the device is intended to be used in the MRI room under physical interaction with the user within a narrow environment, the compliant parts and the output shaft of the device are implemented in a configuration,

in which they are contained in the rigid exterior shell. With such a configuration, the risk of causing any injury to the user due to jamming of body parts into cavities of the device is minimized.

The output shaft connects to the end-effector connector, through holes on the exterior shell that are designed to be larger than required, not to constrain the deflections of the spring up to an extent. The end-effector connector has two functions: to transfer the rotation of the actuator to suitable end-effectors/handles by bypassing the support platform, and to act as a hard stop if the rotation is larger than the workspace limits of the user joint. To implement hard stop limits, the dimensions of end-effector connector are customized based on the range of motion of the targeted joint.

The body of the device is machined from cast-polyamide, a rigid engineering polymer known for its electrical resistance and relatively low weight. This part of the device weights about 3 kg, together with the support platform. Rotating parts of the device weights less than 1.5 kg and have a moment of inertia about 0.01127 kg-m^2.
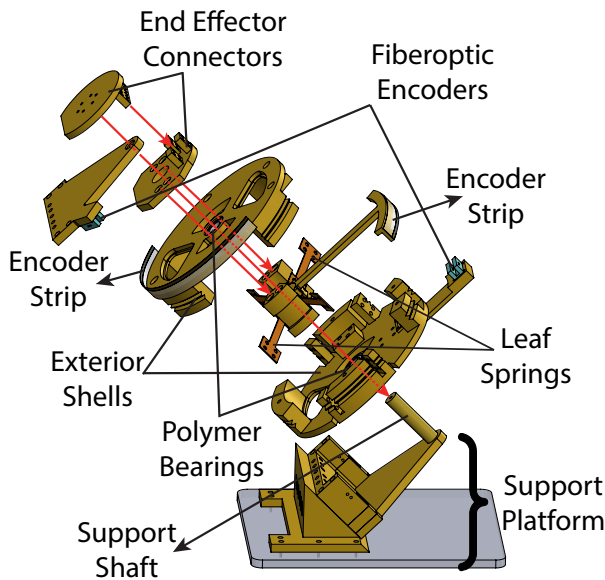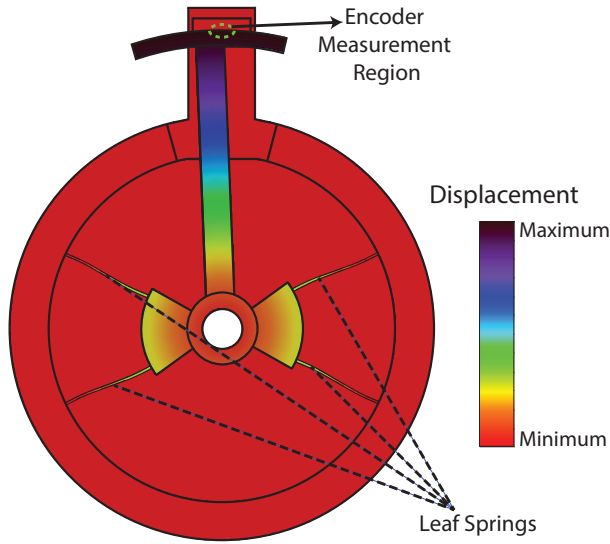

Figure 3. An exploded view of *MRI-VisAct*

Figure 4. Schematic representation of the deflections of the series elastic element and deflection measurements

Series Viscoelastic Element

A series viscoelastic element is implemented to enable MRI compatible force sensing through fiber optic encoder readings. Garolite leaf springs are utilized as compliant elements. Thanks to their geometry in the form of a rectangular plate, leaf springs possess high axial, bending, and torsional stiffness to the forces and torques applied along directions other than the desired direction of deflection. As a consequence, only the bending torques along the direction of the shaft can result in significant deflections of the compliant element, as shown in Figure 4. This way, cross-coupling of forces and moments on the sensor, a parasitic effect suffered by many optical force sensors developed for MR environment (Tan et al. 2011), can be largely avoided.

By adjusting their geometric parameters, the bending stiffness of the leaf springs are designed to be compliant enough to result in large enough deflections that can be measured with sufficient resolution to estimate interaction torques with high fidelity, and large enough to render targeted torque levels and to achieve desired motion/torque control bandwidths from the device. Deflection measurements are performed by an MRI

compatible linear fiber optic encoder attached near the outer diameter of the exterior shell.

As with many polymers, Garolite leaf springs display viscoelastic properties that become more dominant at higher frequencies. Along these lines, we experimentally characterize the viscoelastic behaviour for the leaf springs for use in force estimations during closed-loop torque control.

MRI Compatible Fiber Optic Encoder

Two MRI compatible fiber optic encoders are employed by *MRI-VisAct*, one to measure the rotations of the external shell for precise motion control, and the other to measure the deflections of the leaf springs to estimate interaction torques.

Standard encoders, that position the optical measurement unit and the decoding circuitry in a single compact package, are not preferred for MRI applications, since electrical circuits and metal cables inside MRI room may lead to imaging artifacts and heating, significantly compromising bidirectional compatibility. Consequently, custom fiber optic encoders that avoid any conductive material or electric circuitry within the MRI room are developed. These custom fiber optic encoders, shown in Figure 5, function using the same working principles of a standard quadrature encoder and their signal processing is also performed in a similar manner. The fiber optic encoders consist of light transferring fiber optic cables, an encoder case, an encoder strip within the MRI room, and signal processing elements, fiber optic transmitters (sources) and receivers (sinks) located outside the MRI room.

Commercial fiber optic transmitters and receivers rely on light signals to achieve very high communication rates; hence, they are suitable for high resolution encoder data transmission at kHz update rates. Besides, fiber optic cables can transfer data without significant losses over long distances. Furthermore, fiber optic components featuring plastic/ceramic construction are wide-spread and low-cost.

Straight-tip/physical-contact (ST/PC) cables with a 62.5 μm core diameter are chosen to implement the MRI compatible fiber optic encoders. These cables are available with plastic connection parts, making them suitable for MRI applications. The casing of the encoders are produced from Polyoxymethylene, a non-conductive and MRI compatible material. The casing holds the ceramic ferrules of fiber optic cables in
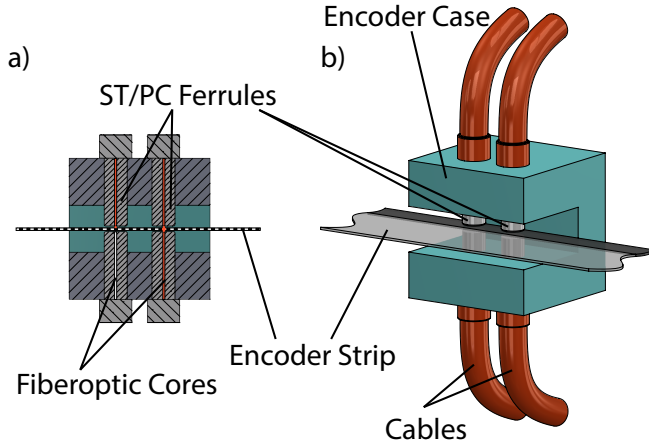
Figure 5. a) Cross-section of the encoder, b) encoder assembly

place with an interference fit, while the encoder strip is positioned in between the ferrules as depicted in Figure 5. Since the distance between lines on the encoder strip should be smaller than the core diameter of the fiber optic cable, 62.5 μm core diameter is suitable with 250-300 line per inch encoder strips. The resolution can further be increased by using a fiber optic cable with a smaller core diameter.

To secure ceramic ferrules with a micrometer precision, two sets of opposing holes are machined on the casing with micro CNC machine. Opposing pairs are machined simultaneously to ensure precise alignment of fiber optic cores for the successful transmission of the light beam. The lateral distance between the centerlines of the hole pairs is chosen to be $(2k \pm 1/2)\, l$ in order to establish a $\pm\pi/2$ phase difference between the A and B signals of the encoder, where l is the length of the transparent and opaque lines of the encoder strip, and k is a positive integer. The lateral alignment of the hole pairs is crucial for performing accurate velocity estimations using encoder readings under quadrature decoding.

Sensor Processing Unit

The sensor processing unit is placed outside the MRI room, since sensor data can be communicated over long distances through fiber optics. The optical signals transmitted to the control room are converted into electrical signals with the help of optical receivers. The processing of these signals is

performed via a series of integrated circuit elements to obtain appropriate signal outputs that can be interfaced with standard commercial encoder decoding modules.

The signals received by the fiber optic receiver are inherently noisy. The main causes for the noise is the open air light transmission. In particular, diffraction occurs in the region where the optic signals exit the transmitter cables, pass through encoder strip, and enter the receiver cable. These multiple diffractions of light causes high frequency oscillations in the electrical signal, which can be captured by the decoder and incorrectly interpreted as instantaneous direction changes of the encoder strip. Even though this noise is bounded by a single encoder count for position readings, its effect on velocity estimations is more extensive.

To reduce the noise, signal processing is implemented in hardware as follows: Firstly, the signal is passed through an RC circuit that acts as a low pass filter. Even though most of the high frequency noise is successfully eliminated by low-pass filtering, remnants of the high frequency oscillations may still be present on the rising or falling edges of the encoder signals. Secondly, a Schmitt Trigger is implemented using a
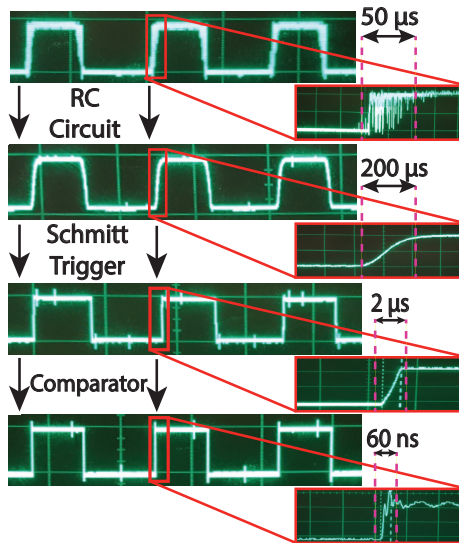

Figure 6. A sample signal processing instance for the MRI compatible fiber optic encoders. Signals between the processing steps are recorded at different time instants; however, the rise and fall behaviors are representative of the signal behavior.

rail to rail op-amp, in order to prevent false readings due to these remnants. Schmitt Trigger acts as a comparator with hysteresis; it not only digitizes the signal, but also hinders low magnitude oscillations from changing the signal reading. Finally, the signal is fed to a high slew rate (5V/80ns) comparator to ensure the rise and fall behaviors are fast enough to be compatible with the velocity estimation modules of commercial encoder decoders, that may perform multiple sampling of a single rising or falling edges with low slew rates. Figure 6 presents a sample signal processing instance for the fiber optic encoders.
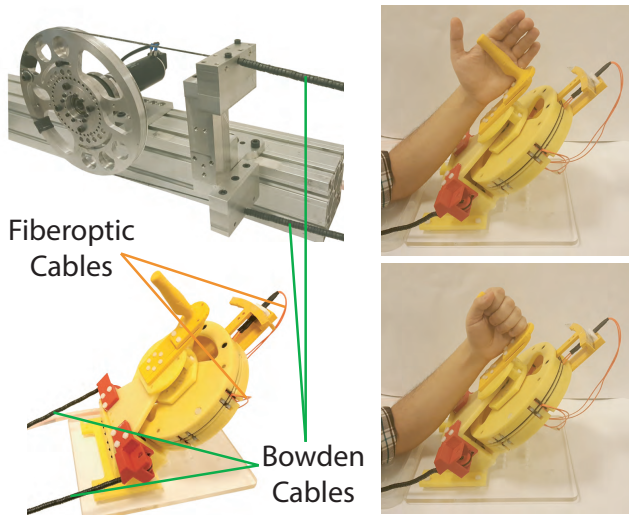

Figure 7. Prototype of *MRI-VisAct*. Left figures show the device with its remote actuation unit, while the right figures present interaction with a user.

Actuation Unit

The actuation unit is placed outside the MRI room, together with the sensing and control equipment. Bowden cables are used to transfer power from geared DC motors to the MRI compatible device. Remote placement of the actuation unit away from the MRI compatible human interface not only ensures bidirectional compatibility, but also significantly reduces the size and weight of the device to be placed within the bore of the MR machine.

The current prototype is presented in Figure 7, where a 200 Watt, coreless, rare magnet DC motor coupled to a harmonic drive with 1:50

transmission ratio is used to actuate the drive pulley. The pulleys have a 1:1 ratio; hence a cumulative transmission ratio of 1:50 is implemented between the external shell of the MRI compatible device and the shaft of the DC motor. The Bowden cable transmission consists of tear-resistant Dyneema ropes and plastic shielding.

Series Elastic Actuation and Torque Control

This section discusses the advantages of series elastic actuation, introduces the model used to capture the viscoelastic behaviour of the compliant element, and reviews the cascaded control architecture used for torque/impedance control of *MRI-VisAct*.

Series Elastic Actuation

MRI-VisAct is powered through a Bowden cable-driven series elastic actuation. This type of actuation has been used in rehabilitation robotics, for instance in (Veneman et al. 2006; Erdogan et al. 2016), to achieve high-fidelity force control with large force output capabilities and to ensure portability of human interface. In this study, in addition to these advantages that ensure that the device possesses a lightweight and portable design with significantly low volume to fit the narrow bore of MRI machines, while simultaneously providing large enough actuation torques required to assist human forearm-wrist, Bowden cable-driven SEA is particularly preferred as it enables bidirectional MRI compatibility, by conveniently placing the controller and actuator units outside the MRI room. Furthermore, revoking the need for high precision and inevitably expensive force sensors, actuators, and transmission elements, SEA helps reduce the cost of *MRI-VisAct*.

Bowden cables and harmonic drive reduction unit of *MRI-VisAct* introduce high friction to the power transmission, resulting in a passively non-backdrivable system. Safety of the patients necessitates reduction of the output impedance of the system, while high fidelity force control is required to adequately assist patients during physical rehabilitation exercises. For low output impedance and high fidelity torque control, series (visco)elastic actuation relies on compliant elements that are intentionally introduced between the Bowden cable-driven exterior shell and the output shaft. In particular, the deliberate introduction of compliance between the Bowden-cable driven actuation unit and the

patient-attached output shaft decouples the high impedance actuator unit from the interface and introduces passive compliance to the system, which acts as a mechanical low pass filter, for instance under impulsive loads and high frequency disturbances, such as torque ripple and stick slip friction originating from the motor/power transmission. Furthermore, the compliant element is also used as the torque sensing unit by measuring its deflections. Compliant elements of series elastic actuators are designed to be orders of magnitude less stiff than commercial force sensors/load cells; hence, these elements experience significantly larger deflections under the interaction forces/torques such that these deflections can be measured using regular position sensors, like optical encoders. Series elastic actuation possesses high-fidelity torque control and active backdrivability within its control bandwidth, while also featuring passive elasticity for excitations above this bandwidth, ensuring safety and robustness throughout the whole frequency spectrum, including hard impacts that may take place (Sensinger and Weir 2006; Erdogan et al. 2016).

Given the inherent performance limitations of force control imposed by non-collocation between the actuator and the force sensor (Eppinger and Seering 1987), series elastic actuation trades-off force-control bandwidth for fidelity, by introducing compliant force/torque sensing elements in the force control scheme (Pratt and Williamson 1995). By decreasing the force sensor stiffness (hence, the system bandwidth), higher force-feedback controller gains can be utilized to achieve responsive and robust force-controllers within the control bandwidth of the system. Robust control is particularly important for Bowden cable driven systems, as the time dependent and nonlinear friction in these cables are highly unpredictable.

The determination of appropriate stiffness of the compliant element is an important aspect of the designs of series elastic actuators, where a compromise solution needs to be reached between force control fidelity, force output capability, and closed-loop bandwidth. In particular, higher compliance can increase force sensing resolution, while higher stiffness can improve the control bandwidth and force output of the system.

Viscoelastic Modeling of the Compliant Element

The compliant elements in series elastic actuators are commonly constructed using metal springs with low hysteresis, such that the force-deflection relationship can be captured algebraically through Hooke's law.

Non-metallic compliant elements has been proposed for use in series elastic actuators to take advantage of their compactness (Austin et al. 2015) and low mass/inertia (Parietti et al. 2011). In this paper, a non-metallic (polymer-based) series elastic element is utilized to maximize the bidirectional MRI compatibility.
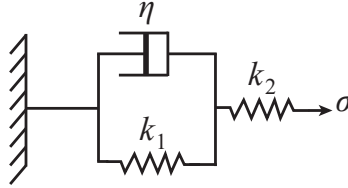

Figure 8. The Standard Linear Model used to capture viscoelastic behaviour of the elastic element

The force-deflection relationship of polymers display viscoelastic properties that become more dominant at higher frequencies. Among the basic models available to capture viscoelastic behaviour, Voigt-Kelvin model excels at modeling an asymptotic deflection behavior under constant force but falls short of modeling instantaneous deflections. Maxwell model can capture instantaneous deflections and creep, but entails infinite deflection under constant force. The combination of these two models, called Burgers model, possesses preferable characteristics of both models. However, this model is overly complicated for modeling the compliant element of *MRI-VisAct* as no creep behavior has been observed in the leaf springs during empirical testing. Along these lines, Standard Linear Model depicted in Figure 8 is used as the underlying viscoelastic model. The Standard Model can account for instantaneous deflections, while also imposing an upper limit on the deflection of the material under constant force.

The force and deflection relationship in the Standard Linear Model is governed by

$$\sigma(t) + \tau_\sigma \, \dot\sigma(t) = M_R \left(\delta(t) + \tau_\delta \, \dot\delta(t) \right)$$
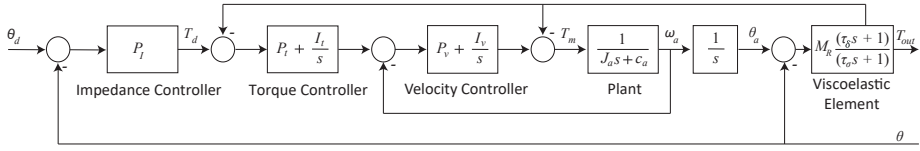
Figure 9. Cascaded controller architecture with inner velocity, intermediate torque, and outer impedance control loops

where σ represents forces and δ denotes deflections. Following definitions hold given the model parameters depicted in Figure 8:

$$\tau_\sigma = \frac{\eta}{k_1 + k_2}$$
$$\tau_\delta = \frac{\eta}{k_1}$$
$$M_R = \frac{k_1 \, k_2}{k_1 + k_2}$$

Torque Control

A real-time cascaded controller is implemented for control of *MRI-VisAct* as shown in Figure 9. In this controller, a fast inner-loop controls the velocity of the outer shell, rendering it into a "ideal" motion source, while an intermediate-loop controls the interaction torque based on the deflection feedback from the compliant element. Finally, an outer-loop can be used for impedance control. The cascaded control architecture is advantageous as it allows for utilization of well-established robust motion controllers for the inner-loop.

In this study, the inner motion control loop is implemented on the motor controller at 10 kHz to compensate for imperfections in the power transmission, such as friction and stiction. The torque and impedance control loops are implemented at 1 kHz. The passivity of the cascaded control architecture of series elastic actuators can be guaranteed with proper choice of controller gains, as demonstrated in (Vallery et al. 2007; Tagliamonte and Accoto 2014).

Experimental Characterization and Verification

This section presents experimental verification of the fiber optic encoders and empirical characterization of the viscoelastic compliant element.

Furthermore, the control performance of *MRI-VisAct* is characterized through a comprehensive set of experiments.

Verification of Fiber Optic Encoders

In order to verify the data gathered using the custom built fiber optic encoders, a series of experiments is conducted during which the performance of the fiber optic encoders is compared to a commercial 250 lines per inch encoder. The encoders are positioned in series such that they read from the same encoder strip.

Arbitrary oscillations up to ± 1000 counts amplitude are applied to the test strip for 180 seconds and data from both encoders are recorded using a real-time I/O control card. Sample data collected during the experiments is given in Figure 10. The RMS error between fiber-optical encoder and commercial encoder is found to be 1.4 counts corresponding to 25 μm, which is likely to be caused by the mechanical coupling and the possible bending of the encoder strip. The results indicate that the custom built encoders achieve the desired level of position measurement performance.
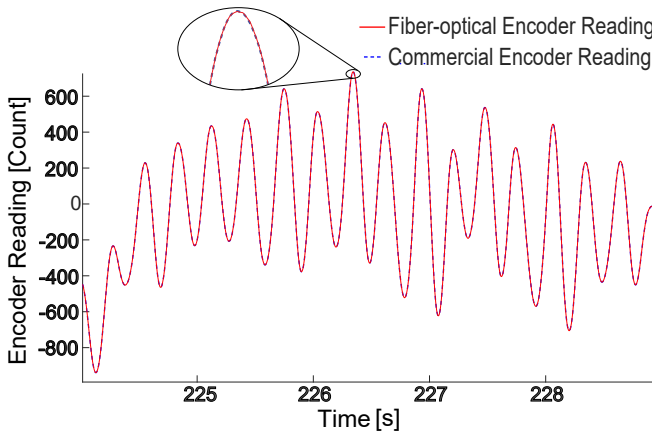

Figure 10. Sample data collected during the encoder verification experiments

Characterization of the Compliant Element

Experimental characterization of the series viscoelastic element is performed using a force/torque sensor rigidly attached to the output shaft. Sinusoidal torque inputs at different frequencies up to 10 Hz are administered to the system over a period of time corresponding to
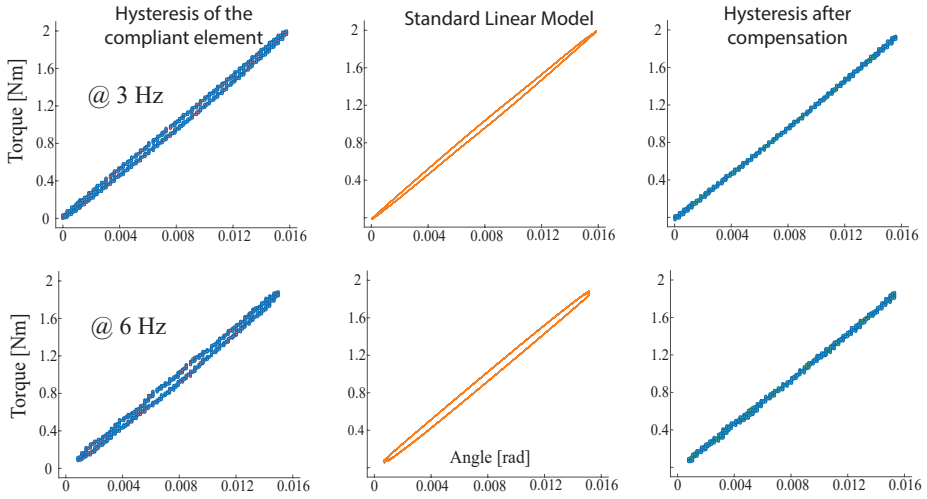
Figure 11. Experimental characterization of the compliant element and hysteresis compensation using the Standard Linear Model for viscoelasticity

at least 30 cycles, during which encoder measurements are recorded. Displacement and torque measurements from these experiments are plotted in Figure 11. Since hysteresis is observed in the results, standard linear model is used to obtain a model for the compliant element.

Identification of the three parameters τ_σ, τ_δ, and M_R of the model is performed in the frequency domain by inspecting the input and output characteristics of sinusoidal signal. Since M_R characterizes the equivalent stiffness of the two springs k_1 and k_2 connected in series, it is identified at low frequency input signals, where the effect of η can be ignored. Once M_R is determined, the remaining model equation becomes linear in τ_σ and τ_δ and these parameters are identified using the phase difference and amplitude ratio of the input and output signals, measured via fiber optic encoder and the torque sensor, respectively. After recording the amplitude ratio and phase shift values for input and output signals for multiple frequencies ranging from 0.1 Hz to 10 Hz, τ_σ and τ_δ have been estimated through a least squares fit, leading to model parameters of k_1=1552 Nm/rad, k_2=135 Nm/rad, and η=38 Nm-s/rad.

The model has been verified at different frequencies to reduce the torque estimation errors due to the hysteresis of the system, as presented in Figure 11. In particular, top row of Figure 11 presents results from

experiments at 3 Hz, while the bottom row presents similar results for 6 Hz. At each frequency, the torque estimation is performed according to Hooke's law and the standard linear model, and these results are compared with the force sensor readings. It has been observed that, for frequencies over 3 Hz, the standard linear model results in 50% reduction in torque estimation error caused by using Hooke's model. The difference between these models is less for frequencies under 3 Hz, where the effects of hysteresis become weaker.

Position Tracking Performance

The dynamic position control performance of *MRI-VisAct* is characterized through a set of experiments. Since the performance of the cascaded control architecture highly relies on the performance of the inner motion control loop, first the position control bandwidth of the device is determined.
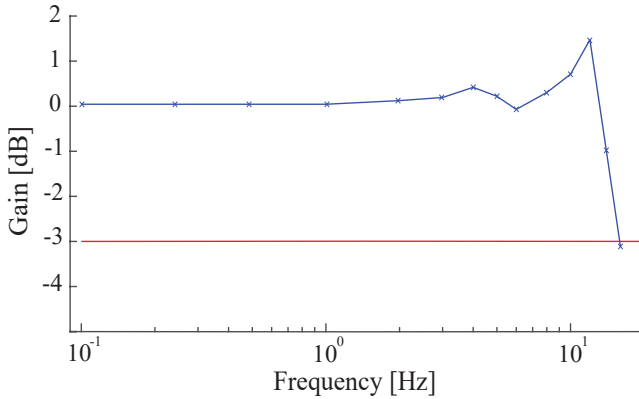

Figure 12. Experimental characterization of the position bandwidth for 5.25° peak-to-peak magnitude sinusoidal inputs

Figure 12 presents the magnitude Bode plot characterizing the position control bandwidth for the system as 15 Hz, for 5.25° peak-to-peak magnitude sinusoidal inputs. Up to this frequency, *MRI-VisAct* can be regarded as a perfect motion source, as necessitated by the outer force and impedance control loops of the cascaded controller. This bandwidth is adequate for series viscoelastic actuation, as the deflections of the elastic element is 5 times lower than 5.25° during normal operation with 2 Nm interaction torque.

The position control bandwidth for $45°$ peak-to-peak magnitude sinusoidal inputs is over 1 Hz, which is also adequate given the bandwidth limitations of patients.

The position tracking performance of *MRI-VisAct* for a chirp motion ranging up to 2 Hz with $30°$ peak-to-peak amplitude is presented in Figure 13. The percent RMS error for this experiment is characterized to stay under 2%.
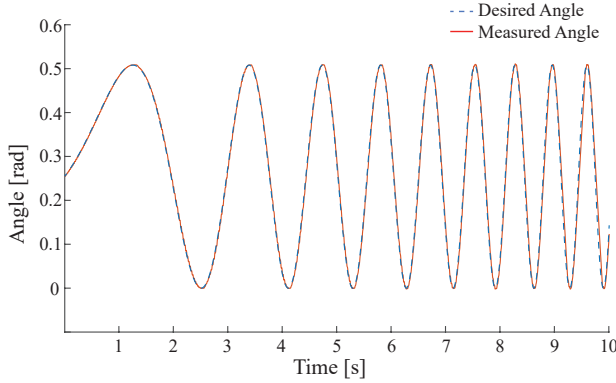

Figure 13. Chirp position reference tracking performance for frequency range up to 2 Hz

Torque Tracking Performance

The dynamic torque control performance of *MRI-VisAct* is presented in Figures 14 and 15. In Figure 14, the set point torque control results are reported for three reference torque values of 1 Nm, 2 Nm and 3 Nm. The steady state torque error for these three references are within the torque sensing resolution, while 10% to 90% rise time and 5% max error settling time are less than 0.09 s and 0.15 s, respectively.

Figure 15 depicts the experimental torque tracking performance of *MRI-VisAct* for a chirp torque reference signal up to 4 Hz with 2 Nm peak-to-peak amplitude. The percent RMS error for this tracking experiment is characterized to stay under 6%.

Figure 16 presents the magnitude Bode plot characterizing the torque control bandwidth as 14 Hz for 2 Nm reference torques, which is sufficiently high to deliver rehabilitation exercises. As expected, the torque control bandwidth of the system gets closer to the position control bandwidth, as reference torque magnitude decreases. These bandwidths may be adjusted by modifying the motion bandwidth of the system.
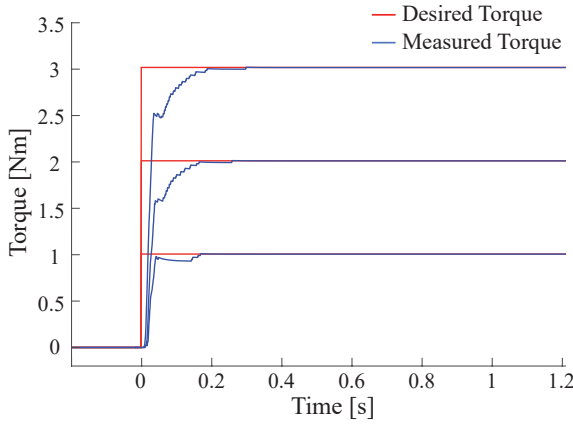
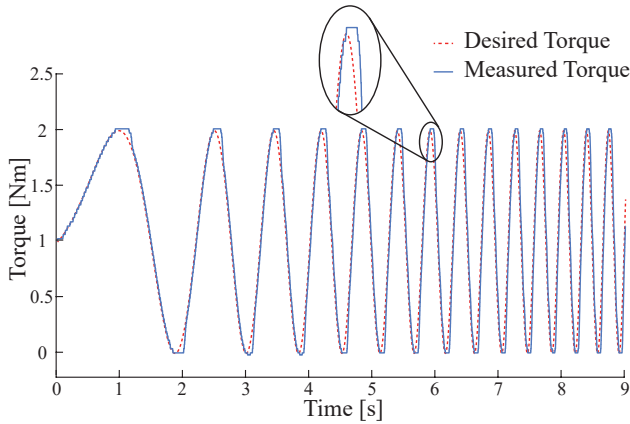**Figure 14.** Set-point torque control performance for reference force values of 1 Nm, 2 Nm, and 3 Nm.

Figure 15. Chirp torque reference tracking performance for a frequency range up to 4 Hz

Alternatively, high force bandwidths is also directly linked to the stiffness of the viscoelastic element and can be altered by modifying the stiffness of the compliant element.

Impedance Rendering Performance

To evaluate the impedance control performance of the device, two virtual fixtures have been rendered as torsional springs with stiffness values of 2.5 Nm/rad and 5 Nm/rad, respectively. Figure 17 presents force-deflection data measured for these renderings, by applying known torques
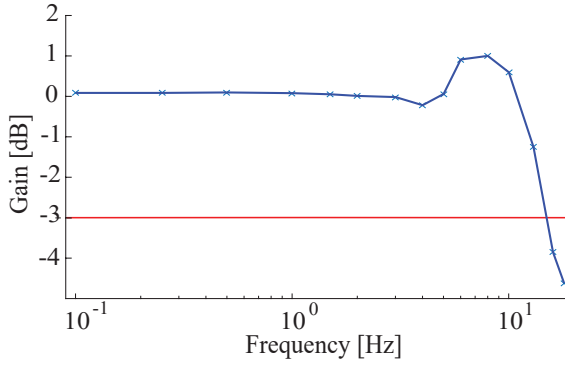
Figure 16. Experimental characterization of the torque control bandwidth with 2 Nm peak-to-peak torque reference

to *MRI-VisAct* and measuring its rotary displacement. Best linear fits on the data are also presented together with R^2 values characterizing the quality of these line fits. These results indicate the device can achieve high fidelity impedance renderings with errors less than 1%.
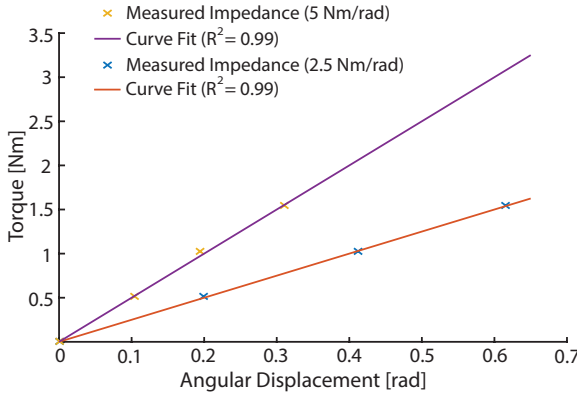

Figure 17. Experimental verification of impedance rendering of two virtual torsional springs with 2.5 Nm/rad and 5 Nm/rad

Discussion and Conclusions

The design, control, and experimental characterization of a Bowden cable-actuated, MRI-compatible series viscoelastic actuator are presented. *MRI-VisAct* features MRI compatible construction, fiber optic sensing units,

and a Bowden cable-based series viscoelastic actuation, such that it can minimize any interference that can cause imaging artifacts during neuro-imaging, and ensure that device performance is not affected by strong magnetic fields.

In (Schueler et al. 1999), bidirectional compatibility of a device with MR environment is evaluated considering five criteria: device movement, device heating, induced electrical currents, image distortion, and device operation. Device movement is due to forces caused by the presence of ferromagnetic materials in an MRI machine. Such forces are not possible with *MRI-VisAct*, since it is constructed using diamagnetic materials. Device heating stems from electromotive forces acting on conductive elements. Given that all the materials within the MRI room are classified as insulators, such heating cannot take place to cause operational dysfunctions and safety hazards. Furthermore, thanks to lack of conductive materials or circuitry inside the MRI room, there is also no risk of inducing currents that can create artifacts on the image. *MRI-VisAct* does not distort the magnetic field outside of its volume, regarding its fully diamagnetic construction. Finally, the performance of the device operation is not affected by the MRI procedure, thanks to remote placement of actuation and control/processing units though use of Bowden cable-based power and fiber optic data transmission.

Even though the current prototype of *MRI-VisAct* is implemented as a single degree of freedom actuator built to administer forearm-wrist exercises, this MRI compatible mechatronic system design is highly customizable and can serve as the building block of higher degrees of freedom MRI compatible robotic devices. In particular, the stiffness of the series viscoelastic element can be customized by simply changing the geometric parameters of the leaf springs, the resolution of the fiber optic encoders can be adjusted by employing fiber optic cables with different core diameters together with encoder strips of appropriate resolution, the workspace of the device can be adjusted though the hard stops on the end-effector connector, while torque output of the device can be adjusted by utilizing more powerful motors and/or higher transmission ratios within the control room.

Acknowledgements

References

J. Austin, A. Schepelmann, and H. Geyer, "Control and evaluation of series elastic actuators with nonlinear rubber springs," in *Intelligent Robots and Systems (IROS), 2015 IEEE/RSJ International Conference on*. IEEE, 2015, pp. 6563–6568.

T. F. Budinger and M. D. Bird, "MRI and MRS of the human brain at magnetic fields of 14t to 20t: Technical feasibility, safety, and neuroscience horizons," *NeuroImage*, 2017.

D. Chapuis, R. Gassert, G. Ganesh, E. Burdet, and H. Bleuler, "Investigation of a cable transmission for the actuation of MR compatible haptic interfaces," in *Biomedical Robotics and Biomechatronics, 2006. BioRob 2006. The First IEEE/RAS-EMBS International Conference on*. IEEE, 2006, pp. 426–431.

Y. Dong, B. H. Dobkin, S. Y. Cen, A. D. Wu, and C. J. Winstein, "Motor cortex activation during treatment may predict therapeutic gains in paretic hand function after stroke," *Stroke*, vol. 37, no. 6, pp. 1552–1555, 2006.

S. Eppinger and W. Seering, "Understanding bandwidth limitations in robot force control," in *IEEE International Conference on Robotics and Automation*, vol. 4. IEEE, 1987, pp. 904–909.

A. Erdogan, B. Celebi, A. C. Satici, and V. Patoglu, "AssistOn-Ankle: A reconfigurable ankle exoskeleton with series-elastic actuation," *Autonomous Robots*, pp. 1–16, 2016.

M. A. Ergin, M. Kühne, A. Thielscher, and A. Peer, "Design of a new MR-compatible haptic interface with six actuated degrees of freedom," in *IEEE RAS & EMBS International Conference on Biomedical Robotics and Biomechatronics*. IEEE, 2014, pp. 293–300.

R. Gassert, L. Dovat, O. Lambercy, Y. Ruffieux, D. Chapuis, G. Ganesh, E. Burdet, and H. Bleuler, "A 2-DoF fMRI compatible haptic interface to investigate the neural control of arm movements," in *IEEE International Conference on Robotics and Automation*, 2006, pp. 3825–3831.

R. Gassert, E. Burdet, and K. Chinzei, "Opportunities and challenges in mr-compatible robotics," *IEEE Engineering in Medicine and Biology Magazine*, vol. 27, no. 3, pp. 15–22, 2008.

M. Hara, G. Matthey, A. Yamamoto, D. Chapuis, R. Gassert, H. Bleuler, and T. Higuchi, "Development of a 2-DoF electrostatic haptic joystick for MRI/fMRI applications," in *IEEE International Conference on Robotics and Automation*, 2009, pp. 1479–1484.

J. Hidler, T. Hodics, B. Xu, B. Dobkin, and L. G. Cohen, "MR compatible force sensing system for real-time monitoring of wrist moments during fMRI testing," *Journal of neuroscience methods*, vol. 155, no. 2, pp. 300–307, 2006.

C. Hollnagel, M. Brügger, H. Vallery, P. Wolf, V. Dietz, S. Kollias, and R. Riener, "Brain activity during stepping: a novel MRI-compatible device," *Journal of Neuroscience Methods*, vol. 201, no. 1, pp. 124–130, 2011.

A. Khanicheh, D. Mintzopoulos, B. Weinberg, A. A. Tzika, and C. Mavroidis, "Evaluation of electrorheological fluid dampers for applications at 3-T MRI environment," *IEEE/ASME Transactions on Mechatronics*, vol. 13, no. 3, pp. 286–294, 2008.

D. Le Bihan, *Looking Inside the Brain: The Power of Neuroimaging*. Princeton University Press, 2014.

S. Li, A. Frisoli, L. Borelli, M. Bergamasco, M. Raabe, and M. W. Greenlee, "Design of a new fMRI compatible haptic interface," in *World Haptics*, 2009, pp. 535–540.

W. S. Lutz, Wolfgang and S. Scherbov, "The coming acceleration of global population ageing," in *Nature, 451(7179)*, 2008, pp. 716–719.

J. P. Mehta, M. D. Verber, J. A. Wieser, B. D. Schmit, and S. M. Schindler-Ivens, "A novel technique for examining human brain activity associated with pedaling using fMRI," *Journal of neuroscience methods*, vol. 179, no. 2, pp. 230–239, 2009.

S. Menon, A. A. Stanley, J. Zhu, A. M. Okamura, and O. Khatib, "Mapping stiffness perception in the brain with an fMRI-compatible particle-jamming haptic interface," in *Annual International Conference of the IEEE Engineering in Medicine and Biology Society*, 2014, pp. 2051–2056.

S. Menon, H. Ganti, and O. Khatib, "Using haptic fMRI to enable interactive motor neuroimaging experiments," in *Experimental Robotics*. Springer, 2016, pp. 89–103.

J. Merlet, *Parallel Robots*, 2nd ed. Springer, 2006.

J. M. Newton, Y. Dong, J. Hidler, P. Plummer-D'Amato, J. Marehbian, R. M. Albistegui-DuBois, R. P. Woods, and B. H. Dobkin, "Reliable assessment of lower limb motor representations with fMRI: Use of a novel MR compatible device for real-time monitoring of ankle, knee and hip torques," *Neuroimage*, vol. 43, no. 1, pp. 136–146, 2008.

F. Parietti, G. Baud-Bovy, E. Gatti, R. Riener, L. Guzzella, and H. Vallery, "Series viscoelastic actuators can match human force perception," *IEEE/ASME Transactions on Mechatronics*, vol. 16, no. 5, pp. 853–860, 2011.

G. Pratt and M. Williamson, "Series elastic actuators," in *IEEE/RSJ International Conference on Intelligent Robots and Systems*, vol. 1, 1995, pp. 399–406.

B. A. Schueler, T. B. Parrish, J.-C. Lin, B. E. Hammer, B. J. Pangrle, E. R. Ritenour, J. Kucharczyk, and C. L. Truwit, "MRI compatibility and visibility assessment of implantable medical devices," *Journal of magnetic resonance imaging*, vol. 9, no. 4, pp. 596–603, 1999.

J. Sensinger and R. Weir, "Improvements to series elastic actuators," in *IEEE/ASME International Conference on Mechatronic and Embedded Systems and Applications*, 2006, pp. 1–7.

Y. M. Senturk and V. Patoglu, "Design and control of an MRI compatible series elastic actuator," in *IEEE International Conference on Robotics and Biomimetics*, 2016.

——, "Manyetik rezonans görüntülemesi uyumlu seri elastik eyleyici tasarımı ve kontrolü," in *Türkiye Otomatik Kontrol Ulusal Toplantısı*, 2016.

F. Sergi, H. I. Krebs, B. Groissier, A. Rykman, E. Guglielmelli, B. T. Volpe, and J. D. Schaechter, "Predicting efficacy of robot-aided rehabilitation in chronic stroke patients using an MRI-compatible robotic device," in *Annual International Conference of the IEEE Engineering in Medicine and Biology Society*. IEEE, 2011, pp. 7470–7473.

F. Sergi, A. C. Erwin, and M. K. O'Malley, "Interaction control capabilities of an MR-compatible compliant actuator for wrist sensorimotor protocols during fMRI," *IEEE/ASME Transactions on Mechatronics*, vol. 20, no. 6, pp. 2678–2690, 2015.

U. Spaelter, D. Chapuis, R. Gassert, R. Moser, and H. Bleuler, "A versatile MRI/fMRI compatible spherical 2-dof haptic interface," in *IEEE/RAS-EMBS International Conference on Biomedical Robotics and Biomechatronics*. IEEE, 2006, pp. 727–732.

N. L. Tagliamonte and D. Accoto, "Passivity constraints for the impedance control of series elastic actuators," *Journal of Systems and Control Engineering*, vol. 228, no. 3, pp. 138–153, 2014.

U. Tan, B. Yang, R. Gullapalli, J. P. Desai *et al.*, "Triaxial MRI-compatible fiber-optic force sensor," *IEEE Transactions on Robotics*, vol. 27, no. 1, pp. 65–74, 2011.

N. Tsagarakis, D. G. Caldwell, and G. A. Medrano-Cerda, "A 7-DoF pneumatic muscle actuator powered exoskeleton," in *IEEE International Symposium on Robot and Human Interactive Communication*, 1999, pp. 327–333.

H. Vallery, R. Ekkelenkamp, H. van der Kooij, and M. Buss, "Passive and accurate torque control of series elastic actuators," in *IEEE/RSJ International Conference on Intelligent Robots and Systems*, 2007, pp. 3534–3538.

J. F. Veneman, R. Ekkelenkamp, R. Kruidhof, F. C. van der Helm, and H. van der Kooij, "A series elastic-and bowden-cable-based actuation system for use as torque actuator in exoskeleton-type robots," *The International Journal of Robotics Research*, vol. 25, no. 3, pp. 261–281, 2006.

P. A. Wolf, R. B. D'Agostino, A. J. Belanger, and W. B. Kannel, "Probability of stroke: A risk profile from the Framingham Study." *Stroke*, vol. 22, no. 3, pp. 312–318, 1991.

A. Yamamoto, K. Ichiyanagi, T. Higuchi, H. Imamizu, R. Gassert, M. Ingold, L. Sache, and H. Bleuler, "Evaluation of MR-compatibility of electrostatic linear motor," in *IEEE International Conference on Robotics and Automation*, 2005, pp. 3658–3663.

N. Yu, C. Hollnagel, A. Blickenstorfer, S. S. Kollias, and R. Riener, "Comparison of MRI-compatible mechatronic systems with hydrodynamic and pneumatic actuation," *IEEE/ASME Transactions on Mechatronics*, vol. 13, no. 3, pp. 268–277, 2008.